Electronic Supplementary Material (ESI) for Physical Chemistry Chemical Physics.

Supplementary Information

Elucidating local diffusion dynamics in nickel-rich layered oxide cathodes

Beth I.J. Johnston,*[a,c] Innes McClelland[a,c], Peter J. Baker [b,c] and Serena A. Cussen *[a,c]

[a]Department of Materials Science and Engineering, The University of Sheffield, Sir Robert Hadfield Building, Sheffield S1 3JD, UK

[b]ISIS Pulsed Neutron and Muon Source, STFC Rutherford Appleton Laboratory, Harwell Science and Innovation Campus, Didcot, OX11 0QX, UK

[c]The Faraday Institution, Quad One, Harwell Science and Innovation Campus, Didcot, OX11 0RA, UK

Static forms of the Kubo-Toyabe function

The zero-field static Kubo-Toyabe function (G_{KT}) is given by

$$G_{KT} = \frac{1}{3} + \frac{2}{3}(1 - \Delta^2 t^2) exp(- \frac{1}{2}\Delta^2 t^2)$$

where Δ is the static field distribution width at the muon stopping site and *t* is the time.[1] Upon an applied longitudinal field, H_{LF}, this can be written as

$$G_{KT} = 1 - \frac{2\Delta^2}{(\gamma_\mu H_{LF})^2}\left(1 - e^{-\frac{1}{2}\Delta^2 t^2}\cos(\gamma_\mu H_{LF} t)\right) + \frac{2\Delta^4}{(\gamma_\mu H_{LF})^3}\int_0^t e^{-\frac{1}{2}\Delta^2 \tau^2} sin(\gamma_\mu H_{LF}\tau)\, d\tau$$

where γ_μ is the muon gyromagnetic ratio and τ is the muon lifetime.[2] However, when ion dynamics are considered, these take a Markovian form with rate ν and a strict analytical form of the dynamic Kubo-Toyabe function is unavailable and the function must be evaluated numerically.[1]

1. Sugiyama, J., Ion Diffusion in Solids Probed by Muon-Spin Spectroscopy. *Journal of the Physical Society of Japan* **2013,** *82* (Suppl.A), SA023.
2. Hayano, R. S.; Uemura, Y. J.; Imazato, J.; Nishida, N.; Yamazaki, T.; Kubo, R., Zero-and low-field spin relaxation studied by positive muons. *Physical Review B* **1979,** *20* (3), 850-859.

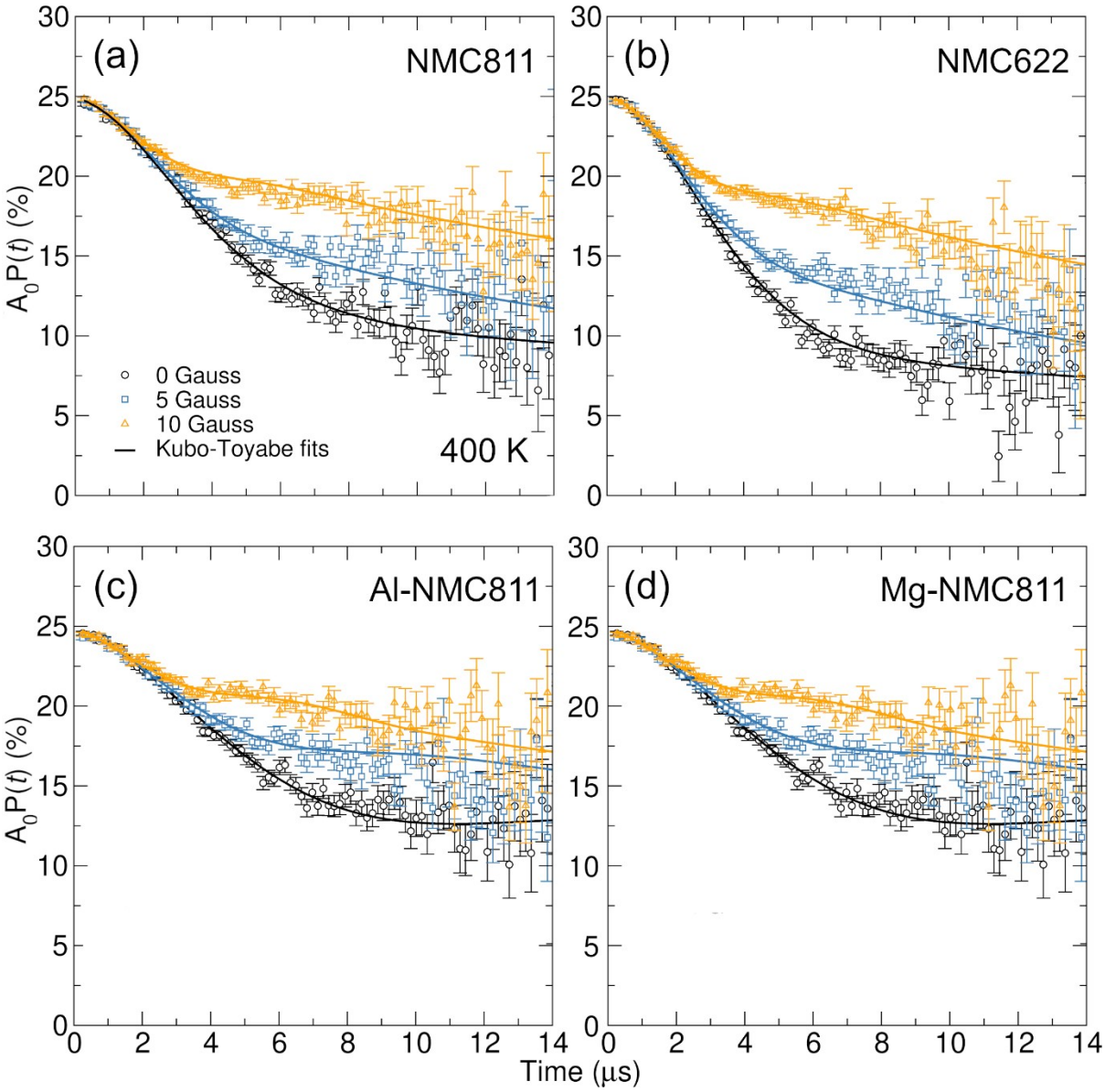

Figure S1. Decay positron asymmetry obtained for μ⁺SR measurements conducted at 400 K for **(a)** NMC811, **(b)** NMC622, **(c)** Al-NMC811 and **(d)** Mg-NMC811 powders. Data at zero field (black circles) and applied longitudinal fields of 5 G (blue squares) and 10 G (orange triangles) are shown alongside fits to the data using the dynamic Kubo-Toyabe function (solid lines).

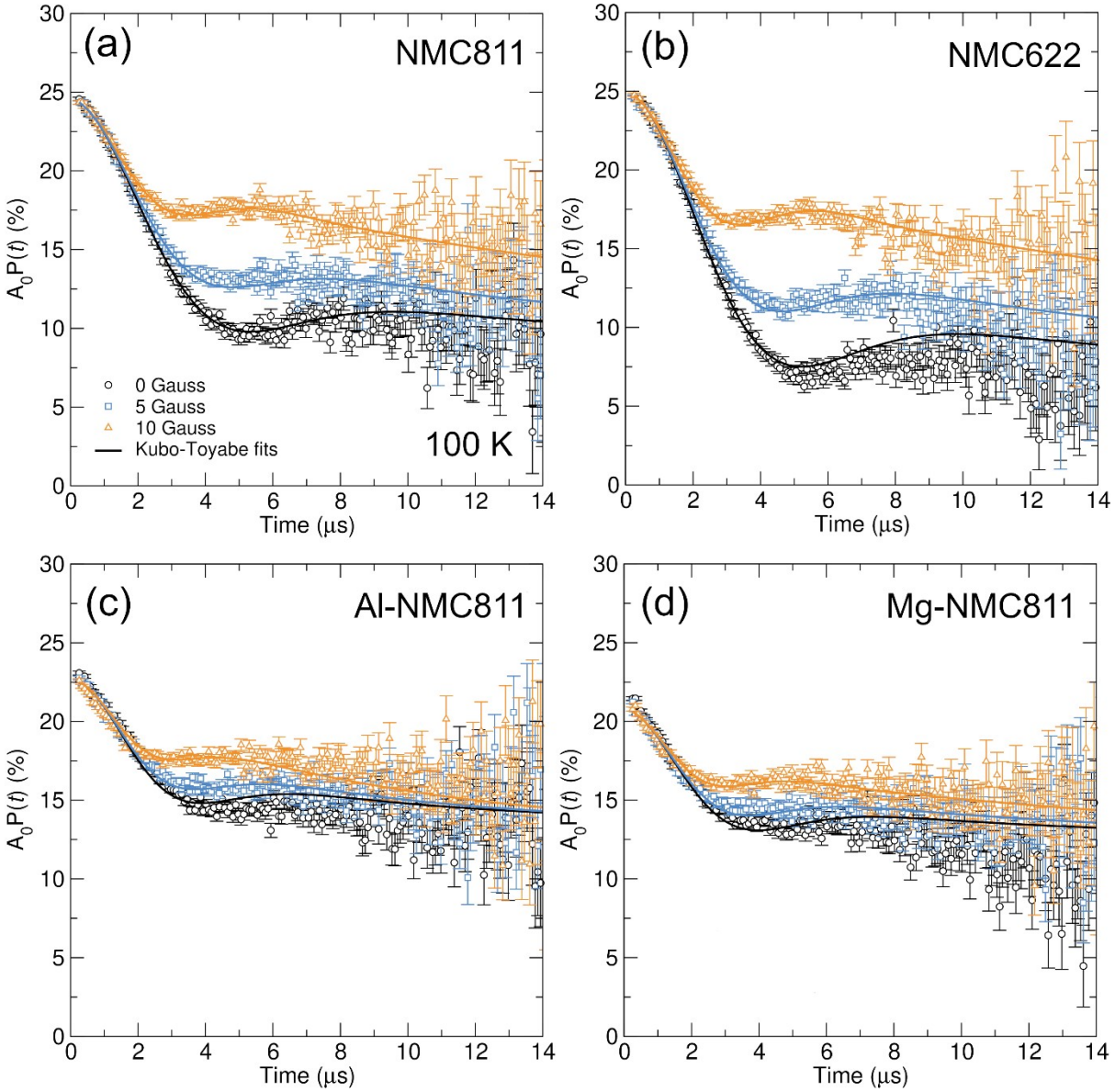

Figure S2. Decay positron asymmetry obtained for μ⁺SR measurements conducted at 100 K for **(a)** NMC811, **(b)** NMC622, **(c)** Al-NMC811 and **(d)** Mg-NMC811 powders. Data at zero field (black circles) and applied longitudinal fields of 5 G (blue squares) and 10 G (orange triangles) are shown alongside fits to the data using the dynamic Kubo-Toyabe function (solid lines).

Table S1. Fitting parameters obtained from μ⁺SR experiments for NMC811. Equation 2 was fit to all three datasets (zero field, 5G and 10 G longitudinal fields) at each temperature point.

Temp (K)	A_{bg}	A_{KT}	Δ (MHz)	ν (MHz)	λ (MHz)	χ^2
100	8.32(6)	15.79(6)	0.356(2)	0.099(2)	0.024(1)	1.051
120	8.35(5)	15.80(6)	0.345(2)	0.092(2)		1.116
140	8.31(6)	16.04(6)	0.339(2)	0.098(3)		0.994
160	8.39(6)	16.02(6)	0.327(2)	0.094(3)		1.193
180	8.54(6)	16.09(6)	0.318(2)	0.086(3)		1.165
200	8.66(6)	16.01(6)	0.310(2)	0.103(3)		1.107
220	8.96(7)	15.79(7)	0.303(2)	0.111(4)		1.035
240	9.06(7)	15.72(7)	0.293(2)	0.125(4)		1.002
260	9.15(8)	15.64(8)	0.281(2)	0.152(3)		1.021
280	9.23(8)	15.57(8)	0.267(2)	0.156(5)		1.06
300	9.49(9)	15.40(9)	0.262(2)	0.178(5)		1.039
320	9.66(10)	15.20(10)	0.257(2)	0.204(6)		1.042
340	9.38(11)	15.52(11)	0.246(2)	0.217(6)		1.019
360	8.80(13)	16.10(12)	0.240(2)	0.239(6)		1.107
380	8.83(14)	16.09(13)	0.235(2)	0.266(7)		1.003
400	8.77(15)	16.06(15)	0.230(2)	0.290(8)		1.012

Table S2. Fitting parameters obtained from μ⁺SR experiments for NMC622. Equation 2 was fit to all three datasets (zero field, 5G and 10 G longitudinal fields) at each temperature point.

Temp (K)	A_{bg}	A_{KT}	ν (MHz)	Δ (MHz)	λ (MHz)	χ^2
100	6.34(6)	18.61(5)	0.081(2)	0.351(2)	0.019(1)	1.299
120	6.38(4)	18.50(5)	0.076(2)	0.355(2)		1.282
140	6.38(4)	18.56(5)	0.081(2)	0.357(2)		1.368
160	6.41(4)	18.60(5)	0.081(2)	0.356(2)		1.38
180	6.41(4)	18.59(5)	0.077(2)	0.348(2)		1.343
200	6.55(5)	18.49(5)	0.075(2)	0.344(2)		1.389
220	6.62(4)	18.38(5)	0.082(2)	0.336(2)		1.342
240	6.63(4)	18.35(5)	0.084(2)	0.330(2)		1.311
260	6.87(4)	18.16(5)	0.091(3)	0.325(2)		1.382
280	6.70(4)	18.32(5)	0.104(3)	0.314(2)		1.287
300	7.08(4)	18.02(5)	0.109(3)	0.310(2)		1.256
320	7.23(4)	17.84(5)	0.132(3)	0.303(2)		1.274
340	7.34(4)	17.75(5)	0.149(4)	0.294(2)		1.257
360	7.65(4)	17.41(6)	0.151(4)	0.286(2)		1.166
380	7.97(4)	17.13(6)	0.168(4)	0.280(2)		1.192
400	7.95(5)	17.14(6)	0.195(5)	0.271(2)		1.11

Table S3. Fitting parameters obtained from μ⁺SR experiments for Al-NMC811. Equation 2 was fit to all three datasets (zero field, 5G and 10 G longitudinal fields) at each temperature point.

Temp (K)	A_{bg}	A_{KT}	ν (MHz)	Δ (MHz)	λ (MHz)	χ^2
100	14.91(4)	7.60(4)	0.103(5)	0.486(3)	0.064(2)	1.887
120	14.83(4)	7.58(4)	0.094(5)	0.470(4)		1.994
140	14.82(5)	8.30(8)	0.098(2)	0.448(11)		1.942
160	14.66(5)	9.03(5)	0.079(4)	0.394(3)		1.91
180	14.58(6)	9.50(6)	0.081(4)	0.363(3)		1.816
200	14.51(6)	9.75(6)	0.078(4)	0.340(3)		1.834
220	14.43(7)	9.94(7)	0.102(5)	0.326(3)		1.726
240	14.24(7)	10.19(7)	0.095(5)	0.313(3)		1.708
260	14.32(8)	10.18(8)	0.105(5)	0.300(3)		1.645
280	14.38(8)	10.12(8)	0.117(6)	0.290(3)		1.372
300	14.48(9)	10.02(9)	0.121(6)	0.277(3)		1.295
320	14.41(10)	10.13(9)	0.139(7)	0.260(3)		1.395
340	14.38(12)	10.19(11)	0.171(8)	0.250(3)		1.231
360	14.28(13)	10.28(13)	0.181(8)	0.238(3)		1.13
380	14.17(15)	10.43(14)	0.213(9)	0.230(3)		1.118
400	14.36(16)	10.18(15)	0.237(10)	0.227(3)		1.057

Table S4. Fitting parameters obtained from μ^+SR experiments for Mg-NMC811. Equation 2 was fit to all three datasets (zero field, 5G and 10 G longitudinal fields) at each temperature point.

Temp (K)	A_{bg}	A_{KT}	ν (MHz)	Δ (MHz)	λ (MHz)	χ^2
100	12.78(3)	8.04(5)	0.072(1)	0.461(3)	0.044(3)	1.614
120	12.81(4)	9.45(5)	0.071(1)	0.403(3)		1.406
140	12.57(3)	11.16(5)	0.081(1)	0.340(2)		1.364
160	12.33(4)	12.03(5)	0.079(1)	0.331(2)		1.31
180	12.28(4)	12.36(5)	0.067(1)	0.313(2)		1.243
200	12.31(4)	12.47(5)	0.072(1)	0.307(2)		1.361
220	12.29(4)	12.59(5)	0.088(1)	0.300(2)		1.362
240	12.38(4)	12.58(5)	0.084(1)	0.288(2)		1.218
260	12.32(4)	12.57(5)	0.091(2)	0.278(2)		1.158
280	12.37(4)	12.52(5)	0.112(5)	0.270(2)		1.124
300	12.67(4)	12.21(6)	0.118(5)	0.264(2)		1.154
320	12.53(5)	12.31(6)	0.127(6)	0.249(2)		1.144
340	12.76(5)	12.01(6)	0.161(7)	0.243(2)		1.068
360	12.57(5)	12.25(6)	0.181(1)	0.231(2)		1.253
380	12.64(5)	12.23(6)	0.189(5)	0.218(2)		1.185
400	12.60(5)	12.28(7)	0.196(6)	0.205(3)		1.099

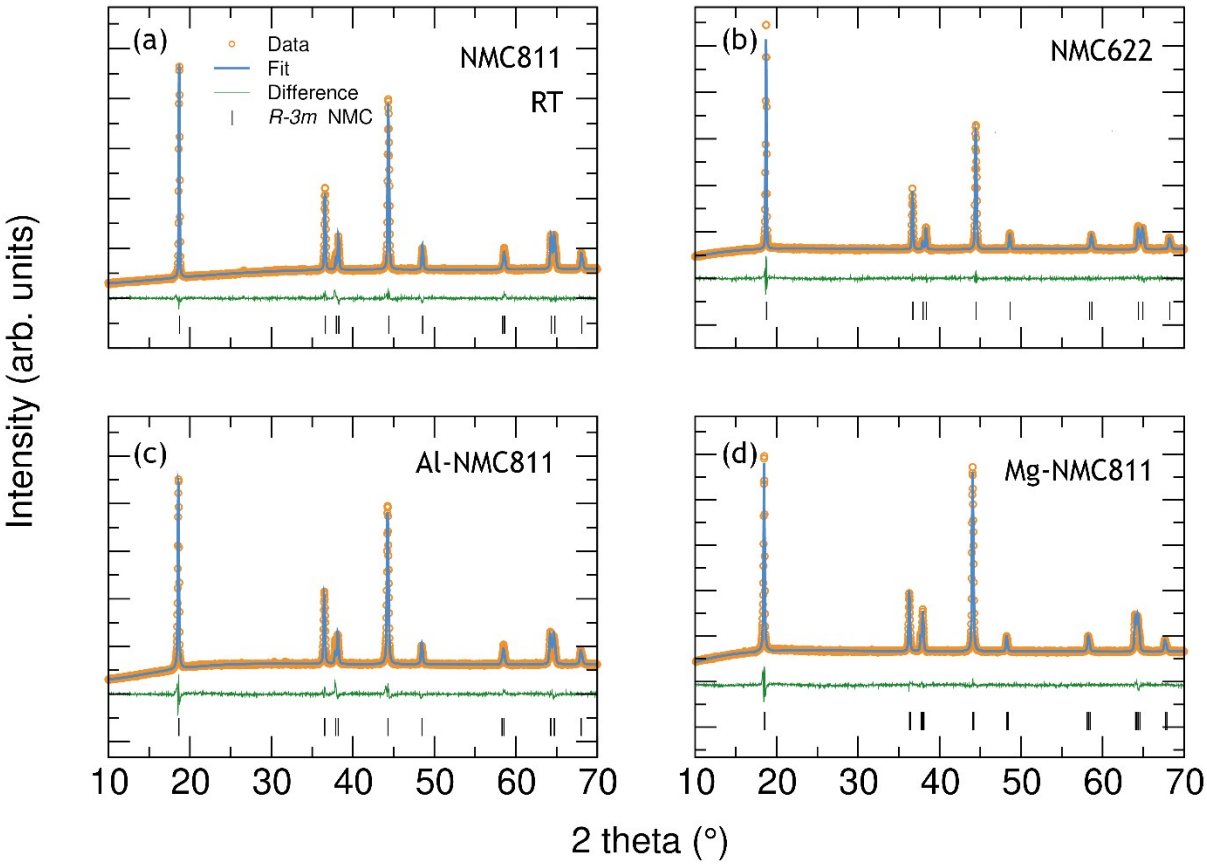

Figure S3. Rietveld refinements on PXRD data obtained at room temperature (RT) from **(a)** NMC811, **(b)** NMC622, **(c)** Al-NMC811 and **(d)** Mg-NMC811.

Table S5. Calculated lattice parameters and Li/Ni mixing values from Rietveld refinements and ratios obtained for NMC811, NMC622, Al-NMC811 and Mg-NMC811 samples.

Sample	**NMC811**	**NMC622**	**Al-NMC811**	**Mg-NMC811**
Space Group	$R\bar{3}m$	$R\bar{3}m$	$R\bar{3}m$	$R\bar{3}m$
***a* (Å)**	2.87784(44)	2.86831(6)	2.87474(22)	2.88061(8)
***c* (Å)**	14.22373(57)	14.21170(18)	14.21257(79)	14.21195(31)
V (Å^3)	102.018(22)	101.258(2)	101.718(14)	102.130(3)
Ni1 occupancy	0.7268(10)	0.5651(10)	0.736(1)	0.738(1)
Ni2 occupancy	0.0732(10)	0.0349(10)	0.054(1)	0.048(1)
***R*$_{wp}$**	2.664 %	2.301 %	3.32%	3.46 %
GOF	1.57	1.45	2.08	2.27

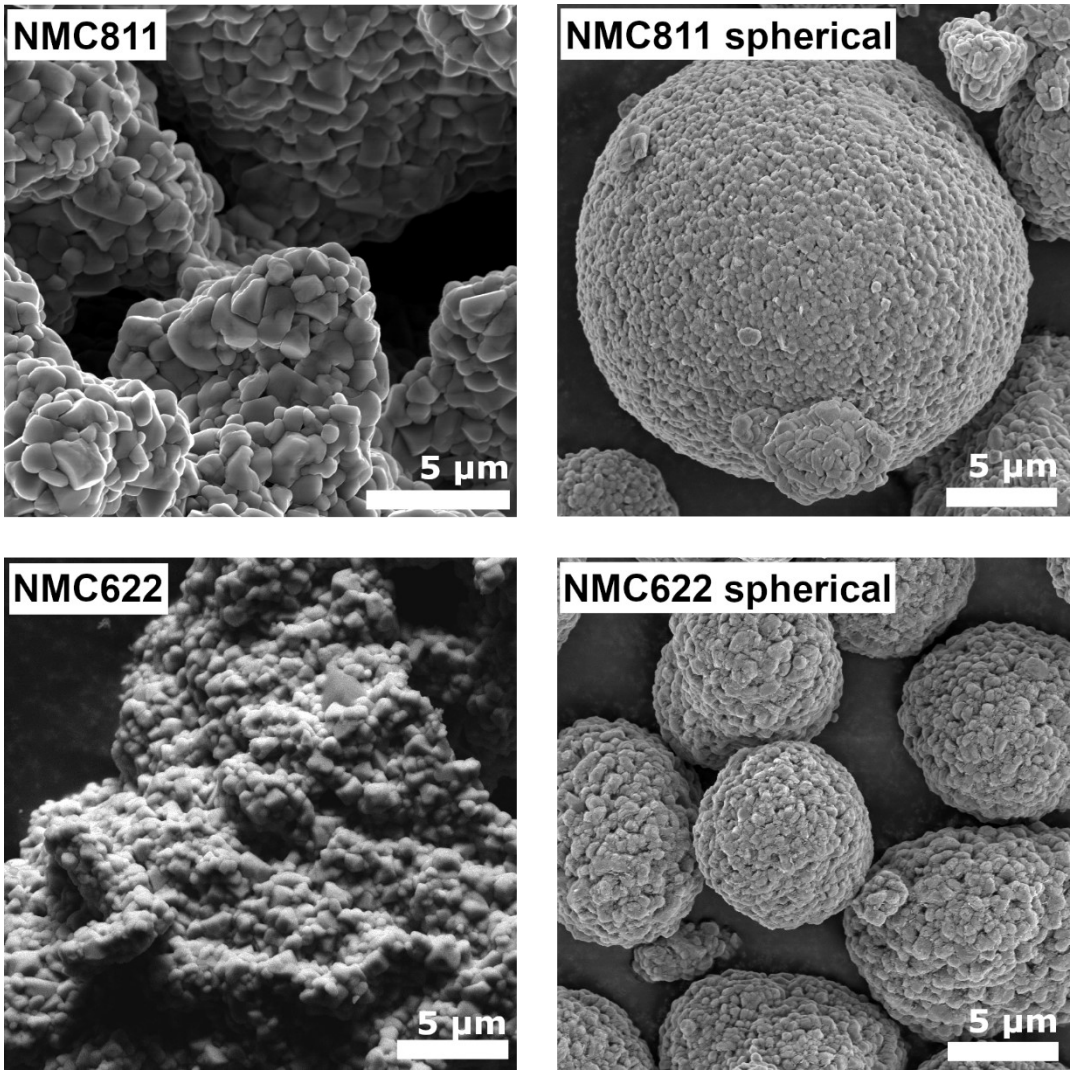

Figure S4. SEM images obtained for NMC811 and NMC622 samples highlighting the different particle morphology observed in microwave-synthesized and commercially supplied powders. SEM images were obtained using an FEI Inspect F50 electron microscope using accelerating voltages of 5 and 10 kV. Samples were prepared on adhesive carbon tabs and coated with Au using a sputter coater to avoid charging feedback.

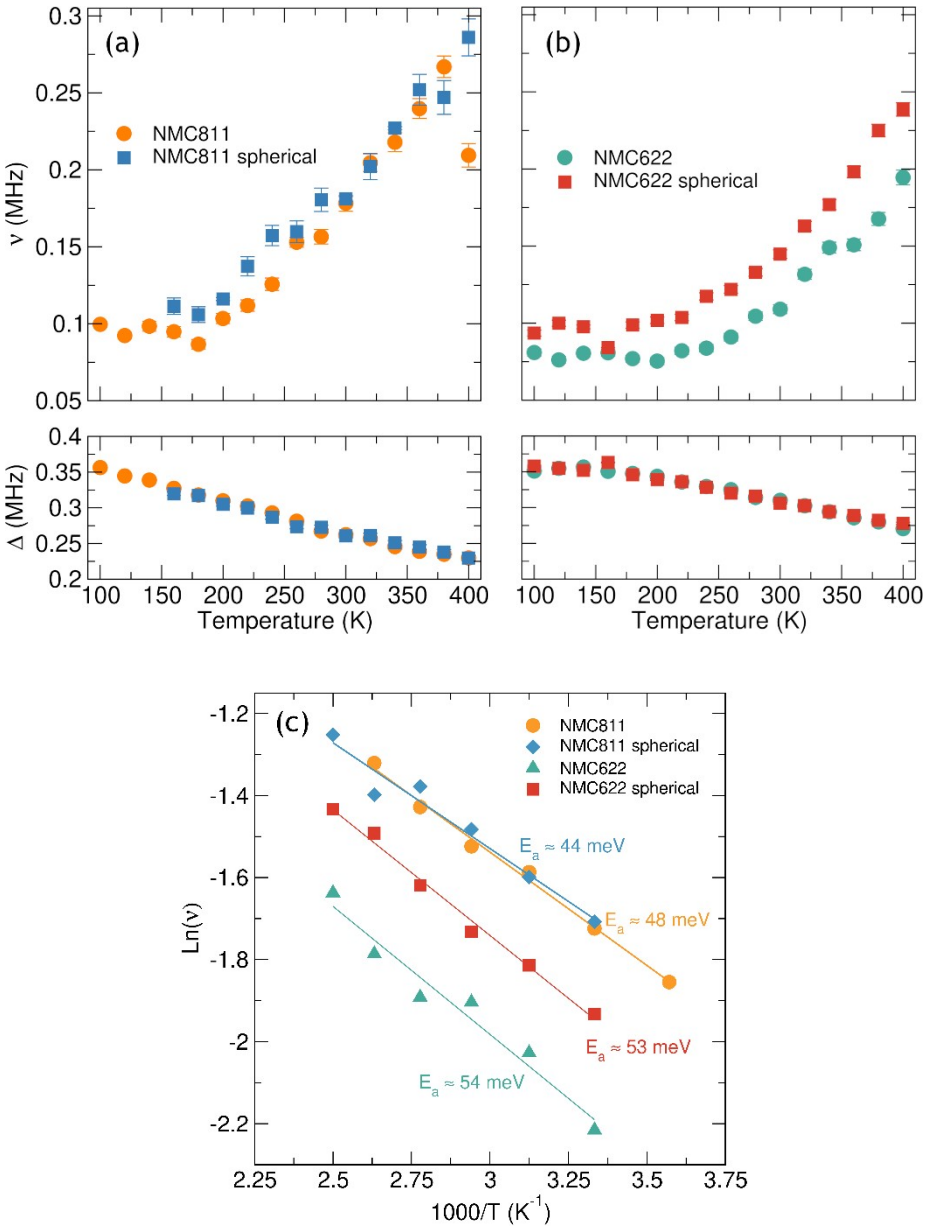

Figure S5. Temperature dependence of the (a) field fluctuation rate (ν) and (b) the local field distribution at the muon stopping site (Δ) for μ⁺SR data collected for the NMC811 and NMC622 samples prepared for this study alongside spherical-shaped NMC811 and NMC822 powders between 100 to 400 K. Arrhenius analysis (c) over the thermally activated region yields the activation energy E_a.

The extracted field fluctuation rates for both NMC811 and spherical NMC811 show very close overlap, indicating that the microscopic Li^+ diffusion for both materials is expected to be very similar, despite the differences in synthesis method and resulting particle morphologies and microstructures, highlighting the muon's independence to meso- and microstructures. Conversely, there is a slight difference between the extracted ν parameters for NMC622 and spherical NMC622. The NMC622 sample consistently shows lower values compared to the spherical samples arising from slower Li^+ diffusion. The higher degree of anti-site mixing in the NMC622 sample (~

2.3 % and 1.9 % for NMC622 and spherical NMC622 respectively as calculated from Rietveld refinements shown in Figure S6 and Table S6) could be causing this effect whereby more Ni^{2+} residing in the Li layer could act to block diffusion pathways and the more highly charged nature of Ni^{2+} compared to Li^{+} could act in a repulsive nature to diffusing Li^{+}, further hindering motion.

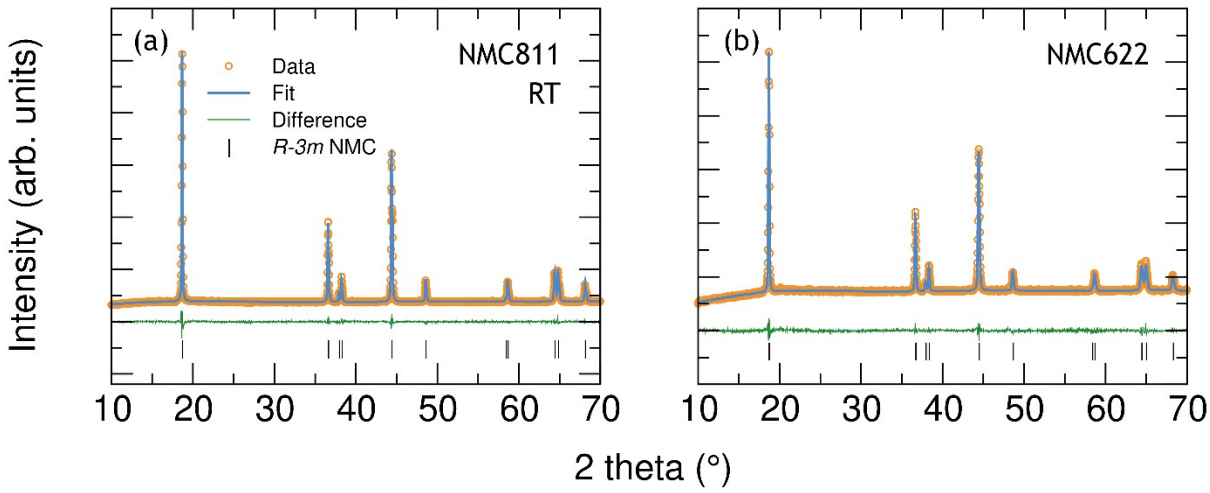

Figure S6. Rietveld refinements on PXRD data obtained at room temperature (RT) from spherical **(a)** NMC811, **(b)** NMC622.

Table S6. Calculated lattice parameters and Li/Ni mixing values from Rietveld refinements and ratios obtained for spherical shaped NMC811 and NMC622 samples.

Sample	**NMC811 spherical**	**NMC622 spherical**
Space Group	$R\bar{3}m$	$R\bar{3}m$
***a* (Å)**	2.87200(5)	2.87075(11)
***c* (Å)**	14.19898(26)	14.22641(57)
V (Å^3)	101.428(3)	101.535(8)
Ni1 occupancy	0.07869(10)	0.5736(10)
Ni2 occupancy	0.0131(10)	0.0264(10)
R_{wp}	2.460 %	1.954 %
GOF	1.59	1.21

Table S7. Values of E_a and D_{Li} at 300 K calculated for NMC811 and NMC622 samples prepared for this study alongside spherical-shaped NMC811 and NMC822 powders as obtained from μ^+SR experiments.

Sample	**E_a (meV)**	**D_{Li} at 300 K ($cm^2\ s^{-1}$)**
NMC811	48 (±2)	$1.6\pm0.1 \times 10^{-11}$
Spherical NMC811	44 (±5)	$1.7\pm0.1 \times 10^{-11}$
NMC622	54 (±6)	$1.0\pm0.1 \times 10^{-11}$
Spherical NMC622	53 (±3)	$1.3\pm0.1 \times 10^{-11}$